

# Forces and atomic relaxations in the pSIC approach with ultrasoft pseudopotentials.

Małgorzata Wierzbowska and Jacek A. Majewski  
*Institute of Theoretical Physics, Faculty of Physics,  
University of Warsaw, ul. Hoża 69, 00-681 Warszawa, Poland*  
(Dated: November 8, 2018)

We present the scheme that allows for efficient calculations of forces in the framework of pseudopotential self-interaction corrected (pSIC) formulation of the density functional theory. The scheme works with norm conserving and also with ultrasoft pseudopotentials and has been implemented in the plane-wave basis code QUANTUM ESPRESSO. We have performed tests of the internal consistency of the derived expressions for forces considering ZnO and CeO<sub>2</sub> crystals. Further, we have performed calculations of equilibrium geometry for LaTiO<sub>3</sub>, YTiO<sub>3</sub>, and LaMnO<sub>3</sub> perovskites and also for Re and Mn pairs in silicon. Comparison with standard DFT and DFT+U approaches shows that in the cases where spurious self-interaction matters, the pSIC approach predicts different geometry, very often closer to the experimental data.

PACS numbers: 31.15.es, 61.50.Ah, 61.72.Bb, 61.72.S-, 71.15.-m

## I. INTRODUCTION

Predictive power of the density functional theory,<sup>1</sup> mostly in its local density (LDA) and gradient corrected (GGA) flavors, is the main factor that has established this method as the standard approach in the materials science. For many electronic systems, it has become possible to predict very accurately the equilibrium geometry, equation of state, relevant energetics, and further whole plethora of properties with astonishingly good accuracy. Unfortunately, all these approximations are plagued by the fact that functionals contain spurious self-interaction and the electronic states are typically too extended. Therefore, the reliable predictions for systems with very localized electronic density, so called strongly-correlated systems, require a computational scheme that cures the self-interaction problem. In some approximate way, the self-interaction is partially removed in the DFT+U scheme,<sup>5</sup> which corrects the Coulomb potential within the localized states, such as *d*- and *f*-shells of atoms. There were also developed methods with the exact exchange,<sup>2-4</sup> and the self-interaction correction (SIC).<sup>6-10</sup> Perhaps the most simple among the DFT+SIC approaches, is the pseudopotential SIC (pSIC) scheme proposed by Filippetti *et al.*<sup>11</sup> Its usefulness to reliably predict energetics has been widely proved in a variety of systems, to mention just a few such as transition metal oxides, manganites and cuprates,<sup>12</sup> diluted magnetic semiconductors (DMSs),<sup>13,14</sup> strongly-correlated superconductors,<sup>15</sup> molecules<sup>16</sup> and molecular junctions,<sup>17</sup> and many other as described in excellent review paper.<sup>12</sup>

Interestingly, the strongly-correlated systems exhibit very often strong deformations of the crystal lattice structures. The interesting and important examples include Jahn-Teller distortions, relaxations around defects, atomic reconstructions at interfaces, lattice distortions due to magnetic interactions, surface reconstructions and local adjustment of atomic positions at surfaces due to the adsorption of atoms and molecules, and finally clusters

of atoms in nanoparticles. It is obvious that the possibility to calculate forces and stress tensor, in addition to the energy spectrum, consistently within the self-interaction free DFT scheme is very desirable.

However, unfortunately, the full equations for forces in the pSIC method have not been set up yet and only an attempt to calculate forces, albeit in a very approximate form, has been performed in the paper by Filippetti and Fiorentini.<sup>12</sup> Even these simplified equations for forces have not been tested so far in any system. Only recently, a new variational pSIC approach,<sup>18</sup> different than the original pSIC approach of Filippetti and Spaldin,<sup>11</sup> has been proposed.

In this work, we provide a computational scheme that is based on the non-variational pSIC method,<sup>11</sup> implementing it into widely used QUANTUM ESPRESSO code<sup>19</sup> using the plane-wave basis and employing ultrasoft pseudopotentials (USPPs).<sup>20</sup> For this scheme, we also derive and implement the formulae for forces. It turns out that the procedure to calculate forces is similar to the one employed in the DFT+U method.<sup>21</sup>

The developed formalism is tested in a series of calculations for various systems. We calculate internal strain parameter *u* for the wurzite ZnO and compare to the DFT+U results for the norm-conserving (NCPP) and the ultrasoft pseudopotentials. We perform tests also for the rare earth compound CeO<sub>2</sub> with *f* valence shells. The relaxations of atomic positions in a cell are also tested for three chosen perovskites in distorted  $P_{nma}$  structure, namely LaTiO<sub>3</sub>, YTiO<sub>3</sub>, and LaMnO<sub>3</sub>. As a third test, we consider pairs of Mn and Re impurities in the silicon lattice, just addressing the problem of transition-metal ions pairing, that is so important for a relevant class of materials, namely the diluted magnetic semiconductors.

The paper is organized as follows: the details of the implementation of the pSIC are given in section II, the full equations for forces are presented in section III, the illustrating implementations of the developed formalism are discussed in section IV, finally, the paper is summarized in section V.

## II. IMPLEMENTATION OF THE PSIC METHOD FOR PLANE-WAVE BASIS COMPUTATIONAL SCHEME

In this section we describe briefly all details necessary to implement the pSIC scheme, just to introduce unique notation necessary for section III. We follow closely formulation from the work by Filippetti *et al.*,<sup>11,12</sup> and collect here the most important equations. Note that the second paper<sup>12</sup> of the authors on this topic differs in some points from the first one,<sup>11</sup> mostly by setting additional simplifications which essentially do not affect accuracy but lead to a speed up of calculations.

In the pSIC method, the Kohn-Sham equation for spin  $\sigma$  orbitals (it implies the usage of a spin-polarized DFT approach) is corrected by the SIC potential  $V_{SIC}$

$$[-\nabla^2 + \hat{V}_{PP} + \hat{V}_{HXC}^\sigma - \hat{V}_{SIC}^\sigma] |\psi_{n\mathbf{k}}^\sigma\rangle = \varepsilon_{n\mathbf{k}}^\sigma |\psi_{n\mathbf{k}}^\sigma\rangle, \quad (1)$$

which is cast in the Kleinman-Bylander form,<sup>22</sup> and contains contributions from the all relevant local orbital potentials related to the local pseudo-orbitals  $\phi_i(\mathbf{r})$  (with index  $i$  describing lumped together angular momentum quantum numbers and position of the atom in the lattice) as follows

$$\hat{V}_{SIC}^\sigma = \sum_i \frac{|\gamma_i^\sigma\rangle\langle\gamma_i^\sigma|}{C_i^\sigma}. \quad (2)$$

The projection operators  $\gamma_i^\sigma$  and the normalization integrands  $C_i^\sigma$  are defined

$$\begin{aligned} \gamma_i^\sigma(\mathbf{r}) &= V_{HXC}^\sigma[n_i^\sigma(\mathbf{r})] \phi_i(\mathbf{r}), \\ C_i^\sigma &= \langle\phi_i| V_{HXC}^\sigma[n_i^\sigma] |\phi_i\rangle. \end{aligned}$$

The  $V_{HXC}^\sigma$  potential is a sum of the Hartree potential and the exchange-correlation potential in a form that results from the DFT functional used in the calculations. The  $V_{HXC}^\sigma$  potential is a functional of the local density  $n_i^\sigma(\mathbf{r})$  that is defined through the atomic pseudo-orbitals  $\phi_i(\mathbf{r})$  and the occupation numbers  $p_i^\sigma$

$$n_i^\sigma(\mathbf{r}) = p_i^\sigma |\phi_i(\mathbf{r})|^2, \quad (3)$$

$$p_i^\sigma = \sum_{n\mathbf{k}} f_{n\mathbf{k}}^\sigma \langle\psi_{n\mathbf{k}}^\sigma|\phi_i\rangle\langle\phi_i|\psi_{n\mathbf{k}}^\sigma\rangle. \quad (4)$$

The occupation numbers  $p_i^\sigma$  are obtained like in the DFT+U scheme from the projection of the Kohn-Sham states  $\psi_{n\mathbf{k}}^\sigma$  onto the local atomic orbitals  $\phi_i$ , and  $f_{n\mathbf{k}}^\sigma$  are the Fermi-Dirac occupations.

Note that if the pseudo-orbital functions do not depend on spin (as in a spin independent PP scheme used throughout this paper), the spin dependence of  $n_i^\sigma(\mathbf{r})$  enters only via the occupation numbers  $p_i^\sigma$ .

It is important to perform orthonormalization of the local pseudo-orbital functions  $\phi_i$  before using them in the above definition of  $p_i^\sigma$ , since it may change considerably the relations between the occupations of different atomic shells. This orthonormalization is not mandatory in the DFT+U method, since this scheme usually involves only one shell of given atom,  $d$ - or  $f$ -shell, but not the both.

Further, the pSIC potential is scaled by one half for the relaxation contribution in the extended systems<sup>11</sup>

$$V_{HXC}^\sigma[n_i^\sigma] \rightarrow \frac{1}{2} V_{HXC}^\sigma[n_i^\sigma]. \quad (5)$$

In general, the scaling coefficient is applied in this place to unify the bulk and molecular systems.<sup>12,16</sup>

In order to simplify calculations, two approximations are made for the pSIC potential:

1) The first assumption is the linear dependence of  $V_{HXC}$  on the occupation numbers

$$V_{HXC}^\sigma[n_i^\sigma] = p_i^\sigma V_{HXC}^\sigma[n_i^\sigma; p_i^\sigma = 1]. \quad (6)$$

Above procedure is exact for the Hartree part of the potential, but it is approximate for the much smaller exchange-correlation part. In this point the orbital exchange-correlation potential has to be calculated with fully spin polarized orbital density.

2) The second simplification assumes employing the spherically averaged radial local orbital density  $n_i^\sigma(r)$  to compute the local orbital potential  $V_{HXC}^\sigma$ .

Therefore, the angular part characterized by quantum number  $m_l$  of pseudo-orbitals is used only to calculate  $p_i^\sigma$  and  $C_i^\sigma$  as follows

$$\begin{aligned} \gamma_{I,m_l,l}^\sigma(\mathbf{r}) &= \frac{1}{2} p_{I,m_l,l}^\sigma V_{HXC}^\sigma[n_{I,l}^\sigma(r); 1] \phi_{I,m_l,l}^\sigma(\mathbf{r}), \\ C_{I,m_l,l}^\sigma &= \frac{1}{2} p_{I,m_l,l}^\sigma \int d\mathbf{r} V_{HXC}^\sigma[n_{I,l}^\sigma(r); 1] (\phi_{I,m_l,l}^\sigma(\mathbf{r}))^2, \end{aligned}$$

where the indices  $m_l$  denote the angular momentum quantum number of the shell  $l$  ( $s$ ,  $p$ ,  $d$ , or  $f$ ) of the atom of type  $I$ .

The total energy within the non-variational spin polarized pSIC scheme is constructed to resemble the DFT one and reads

$$\begin{aligned} E_{SIC}[n, m] &= \sum_{i,\sigma} f_{n\mathbf{k}}^\sigma \varepsilon_{n\mathbf{k}}^\sigma + E_{ion} - \\ &\sum_{\sigma} \int d\mathbf{r} n^\sigma(\mathbf{r}) V_{HXC}^\sigma[n(\mathbf{r}), m(\mathbf{r})] + E_{HXC}[n(\mathbf{r}), m(\mathbf{r})] - \\ &\sum_{i,\sigma} E_{HXC}[n_i^\sigma] + \sum_{n\mathbf{k},\sigma} f_{n\mathbf{k}}^\sigma \langle\psi_{n\mathbf{k}}^\sigma|\hat{V}_{SIC}^\sigma|\psi_{n\mathbf{k}}^\sigma\rangle, \end{aligned} \quad (7)$$

where  $n(\mathbf{r})$  and  $m(\mathbf{r})$  are the total and the spin polarization density, respectively.

The exchange-correlation part of the total energy correction is a small number defined as

$$E_{HXC}[n_i^\sigma] = \int d\mathbf{r} n_i^\sigma(\mathbf{r}) \left( \frac{1}{2} V_H[n_i^\sigma(\mathbf{r})] + \varepsilon_{XC}[n_i^\sigma(\mathbf{r})] \right),$$

where  $\varepsilon_{XC}$  is the local exchange-correlation energy density.

The last term in the formula (7) is the band correction, and shifts the total energy very strongly, restoring its proper curvature with respect to a change of the lattice constant (see Fig. 7 in Ref. [11]).

In the scheme presented here, we implement equations for the ultrasoft pseudopotentials,<sup>20</sup> since they allow for substantial reduction of the energy cutoff for systems consisting of transition metals and rare earth atoms. However, the USPP are not norm-conserving and need some additional terms to be included in the ordinary DFT and the pSIC methods. These terms contain the augmented charges  $Q_{\alpha\alpha'}$  and projectors  $\beta_\alpha$ . The overlap matrix for an orthonormality condition is

$$\hat{S} = \hat{1} + \sum_{\alpha\alpha'} |\beta_\alpha\rangle q_{\alpha\alpha'} \langle\beta_{\alpha'}|, \quad (8)$$

where

$$q_{\alpha\alpha'} = \int d\mathbf{r} Q_{\alpha\alpha'}(\mathbf{r})$$

$$Q_{\alpha\alpha'}(\mathbf{r}) = \phi_\alpha^{AE}(\mathbf{r})\phi_{\alpha'}^{AE}(\mathbf{r}) - \phi_\alpha^{PS}(\mathbf{r})\phi_{\alpha'}^{PS}(\mathbf{r}),$$

$\phi_\alpha^{AE}$  and  $\phi_\alpha^{PS}$  are the all-electron and the pseudo-atomic functions, and  $\alpha = [n, l, m, I]$  sets all quantum numbers for the atom  $I$ .

The pseudopotential splits into the local part  $V_{LOC}(\mathbf{r})$  and the non-local part  $D_{\alpha\alpha'}^\sigma$ , which consists of the Kleinman-Bylander term  $\tilde{D}_{\alpha\alpha'}^\sigma$  and the augmentation term as follows

$$D_{\alpha\alpha'}^\sigma = \tilde{D}_{\alpha\alpha'}^\sigma + \int d\mathbf{r} (V_{LOC}(\mathbf{r}) + V_{HXC}^\sigma(\mathbf{r})) Q_{\alpha\alpha'}(\mathbf{r}).$$

With the above definitions, the pSIC orbital density is

$$n_i^\sigma(\mathbf{r}) = p_i^\sigma ( |\phi_i(\mathbf{r})|^2 + \sum_{\alpha\alpha'} \langle\phi_i^\sigma|\beta_\alpha\rangle Q_{\alpha\alpha'}(\mathbf{r}) \langle\beta_{\alpha'}|\phi_i^\sigma\rangle ),$$

and the pSIC-USPP occupation numbers are

$$p_i^\sigma = \sum_{n\mathbf{k}} f_{n\mathbf{k}}^\sigma \langle\psi_{n\mathbf{k}}^\sigma|\phi_i\rangle \langle\phi_i|\psi_{n\mathbf{k}}^\sigma\rangle \times$$

$$[ 1 + \sum_{\alpha\alpha'} \langle\phi_i^\sigma|\beta_\alpha\rangle q_{\alpha\alpha'} \langle\beta_{\alpha'}|\phi_i^\sigma\rangle ]$$

$$= \sum_{n\mathbf{k}} f_{n\mathbf{k}}^\sigma \langle\psi_{n\mathbf{k}}^\sigma|\hat{S}\phi_i\rangle \langle\phi_i\hat{S}^*|\psi_{n\mathbf{k}}^\sigma\rangle.$$

The pSIC potential within the USPP scheme contains an additional term which reads

$$\hat{V}_{US}^\sigma = \sum_i \frac{1}{2} p_i^\sigma \sum_{\alpha\alpha'} |\beta_\alpha\rangle \langle\beta_{\alpha'}| \times$$

$$\left( \int d\mathbf{r} V_{HXC}^\sigma[n_i^\sigma(\mathbf{r}); 1] Q_{\alpha\alpha'}(\mathbf{r}) \right).$$

Thus, the Kohn-Sham equation with the USPP is

$$[-\nabla^2 + \hat{V}_{LOC} + \hat{V}_{HXC}^\sigma + \sum_{\alpha\alpha'} |\beta_\alpha\rangle D_{\alpha\alpha'}^\sigma \langle\beta_{\alpha'}| -$$

$$(\hat{V}_{SIC}^\sigma + \hat{V}_{US}^\sigma)] |\psi_{n\mathbf{k}}^\sigma\rangle = \varepsilon_{n\mathbf{k}}^\sigma \hat{S} |\psi_{n\mathbf{k}}^\sigma\rangle.$$

The total energy terms of the pSIC origin are

$$-\sum_{i,\sigma} E_{HXC}[n_i^\sigma] + \sum_{n\mathbf{k}} f_{n\mathbf{k}}^\sigma \langle\psi_{n\mathbf{k}}^\sigma| (\hat{V}_{SIC}^\sigma + \hat{V}_{US}^\sigma) |\psi_{n\mathbf{k}}^\sigma\rangle. \quad (9)$$

In addition, the pSIC equations in the covariant form contain the off-diagonal occupation numbers

$$p_{I,m_l,m'_l,l}^\sigma = \sum_{n\mathbf{k}} f_{n\mathbf{k}} \langle\psi_{n\mathbf{k}}^\sigma| \hat{S} \phi_{I,m_l,l}\rangle \langle\phi_{I,m'_l,l}|\hat{S}^*|\psi_{n\mathbf{k}}^\sigma\rangle,$$

$$V_{SIC}^\sigma = \sum_{I,m_l,m'_l,l} \frac{|\gamma_{I,m_l,l}\rangle \frac{1}{2} p_{I,m_l,m'_l,l}^\sigma \langle\gamma_{I,m'_l,l}|}{C_{I,m_l,l}^{1/2} C_{I,m'_l,l}^{1/2}}$$

$$\gamma_{I,m_l,l} = V_{HXC}[n_{I,l}(r); 1] \phi_{I,m_l,l}(r)$$

$$C_{I,m_l,l} = \int d\mathbf{r} \phi_{I,m_l,l}(\mathbf{r}) V_{HXC}[n_{I,l}(r); 1] \phi_{I,m_l,l}(\mathbf{r}).$$

Another approximation for the augmentation part of the pSIC potential is made, assuming that the chosen pseudo-orbitals form a complete basis set. Thus, the beta projectors act on the atomic radial functions and enable simple calculation of the radial integrals. Later, the Kohn-Sham states are projected onto the pseudo-orbitals in the plane-wave representation, as it is a case in the occupation numbers. The corresponding definitions are following

$$\hat{V}_{US}^\sigma = \sum_{I,m'_l,m_l,l} |\hat{S} \phi_{I,m_l,l}\rangle \times$$

$$\frac{1}{2} p_{I,m_l,m'_l,l}^\sigma \varepsilon_{I,m'_l,m_l,l}^{aug} \langle\phi_{I,m_l,l}|\hat{S}^*|,$$

and

$$\varepsilon_{I,m_l,m'_l,l}^{aug} = \sum_{\alpha\alpha'} \langle\phi_{I,m_l,l}|\beta_\alpha\rangle \times$$

$$\int d\mathbf{r} V_{HXC}^\sigma[n_{I,l}(r); 1] Q_{\alpha\alpha'}(\mathbf{r}) \langle\beta_{\alpha'}|\phi_{I,m'_l,l}\rangle.$$

In the above form, the  $\hat{V}_{US}^\sigma$  potential is computation-ally as simple as the occupation numbers, because the quantities  $\varepsilon_i^{aug}$  depend only on the pseudopotential parameters and can be calculated ones.

### III. FORCES IN THE PSIC SCHEME

In this section, we give complete equations for forces in the pSIC scheme with ultrasoft pseudopotentials.

According to the Hellman-Feynman theorem, the forces contain only the derivatives of the potentials and not the Bloch functions. The  $\alpha$  index denotes one of the cartesian directions  $x, y, z$  from now on, and the  $\alpha$  component of the displacement of atom  $I$  is denoted as  $\tau_{\alpha,I}$ .

Thus, following the equation (9), we get an expression for the pSIC contribution to forces

$$F_{\alpha,I}^{SIC} = -\frac{\partial E_{SIC}}{\partial \tau_{\alpha,I}} = \sum_{m_i,l,\sigma} \frac{\partial E_{HXC}[n_{I,m_i,l}^\sigma]}{\partial \tau_{\alpha,I}} - \sum_{n,\mathbf{k}} f_{n\mathbf{k}}^\sigma \left[ \left\langle \psi_{n\mathbf{k}}^\sigma \left| \frac{\partial V_{SIC}}{\partial \tau_{\alpha,I}} \right| \psi_{n\mathbf{k}}^\sigma \right\rangle + \left\langle \psi_{n\mathbf{k}}^\sigma \left| \frac{\partial V_{US}}{\partial \tau_{\alpha,I}} \right| \psi_{n\mathbf{k}}^\sigma \right\rangle \right].$$

The explicit derivatives are:

$$\begin{aligned} \frac{\partial E_{HXC}[n_{I,m_i,l}^\sigma]}{\partial \tau_{\alpha,I}} = & \\ 2 \int d\mathbf{r} p_{I,m_i,m_i',l}^\sigma \frac{\partial p_{I,m_i,m_i',l}^\sigma}{\partial \tau_{\alpha,I}} [n_{I,m_i,l}(\mathbf{r}); 1] \times & \\ \left( \frac{1}{2} V_H[n_{I,l}(\mathbf{r}); 1] + \varepsilon_{XC}[n_{I,l}(\mathbf{r}); 1] \right) & \end{aligned} \quad (10)$$

and

$$\begin{aligned} \frac{\partial V_{SIC}}{\partial \tau_{\alpha,I}} = \frac{1}{2} \sum_{m_i,m_i',l,\sigma} C_{I,m_i,l}^{-1/2} C_{I,m_i',l}^{-1/2} \times & \\ \left[ |\gamma_{I,m_i,l}\rangle \frac{\partial p_{I,m_i,m_i',l}^\sigma}{\partial \tau_{\alpha,I}} \langle \gamma_{I,m_i',l}| + \right. & \\ \left. \frac{\partial \gamma_{I,m_i,l}}{\partial \tau_{\alpha,I}} \right] p_{I,m_i,m_i',l}^\sigma \langle \gamma_{I,m_i',l}| + c.c. \quad & \end{aligned} \quad (11)$$

and the ultrasoft part

$$\begin{aligned} \frac{\partial V_{US}}{\partial \tau_{\alpha,I}} = \frac{1}{2} \sum_{m_i',m_i'',l,\sigma} \varepsilon_{I,m_i',m_i'',l}^{aug} & \\ \left[ |\hat{S}\phi_{I,m_i,l}\rangle \frac{\partial p_{I,m_i,m_i',l}^\sigma}{\partial \tau_{\alpha,I}} \langle \hat{S}^* \phi_{I,m_i'',l}| + \right. & \\ \left. \frac{\partial \langle \hat{S}\phi_{I,m_i,l}|}{\partial \tau_{\alpha,I}} \right] p_{I,m_i,m_i',l}^\sigma \langle \hat{S}^* \phi_{I,m_i'',l}| + c.c. \quad & \end{aligned} \quad (12)$$

The derivatives  $\frac{\partial p_{I,m_i,m_i',l}^\sigma}{\partial \tau_{\alpha,I}}$  and  $|\partial \langle \hat{S}\phi_{I,m_i,l}| / \partial \tau_{\alpha,I}\rangle$  are defined in Ref. [21] by eqs. (13-19), and we give them explicitly in the appendix. The derivative  $|\partial \gamma_{I,m_i,l} / \partial \tau_{\alpha,I}\rangle$  is obtained in the same way as the derivative  $|\partial \langle \hat{S}\phi_{I,m_i,l}| / \partial \tau_{\alpha,I}\rangle$ , because the potential  $V_{HXC}[n_{I,l}(r)]$  moves together with the atomic functions.

For the derivative of the overlap operator  $\hat{S}$ , the following approximation is made. It is assumed that contributions of the beta functions centred at the atoms different than the moved atom are neglected. It turns out that this approximation does not corrupt the accuracy, and it will be shown in the test cases later on. This simplification is necessary, because in the pSIC scheme the projectors used in the definition of the occupation numbers have to be orthogonalized, which in turn sets a difficulty in calculation of the derivatives.

Above definitions are valid for the non-variational pSIC approach. First approximate equations for forces have been given by Filippetti and Fiorentini,<sup>12</sup> however their formulae neglected terms with the derivatives of the occupation numbers. Recent work by Filippetti *et al.*<sup>18</sup> for the variational pSIC scheme contains similar expressions for forces. We have added the derivatives of occupation numbers in a way akin to the equations for forces in the DFT+U scheme.<sup>21</sup> These terms are rather small, and we show their effect discussing the CeO<sub>2</sub> case in the next section.

### IV. TESTS FOR FORCES AND RELAXATIONS

#### A. Wurzite ZnO and CeO<sub>2</sub> in the $F_{m3m}$ structure

As a first test case, we employ introduced scheme for forces to the wurzite ZnO. We use the ultrasoft pseudopotential, the LDA exchange-correlation functional in the parametrization of Perdew-Zunger, the kinetic energy cutoff of 35 Ry, and the uniform Monkhorst-Pack (6,6,6) k-mesh in these calculations.

The results for the total energy and the force acting on the displaced atom Zn(1) in the wurzite unit cell are presented in Figure 1. The Zn atom is displaced only in the  $z$ -direction and the magnitude of the displacement is given as a function of Wyckoff position in units of the lattice constant.

First, we discuss the role of the approximation simplifying the orthogonalization of local atomic projectors on the total energy vs. atomic displacement curves and forces for both LDA+U and pSIC methods. As we have mentioned in the section III, in this approximation the non-local contributions of beta functions to the derivatives are neglected, and only the diagonal terms in the beta functions are considered when the derivative with respect to the atomic position is calculated. The LDA+U

calculations (with  $U=5$  eV) with non-orthogonalized projectors, called "atomic", are performed without any approximation. Simultaneously, calculations of the approximate forces obtained with the orthogonalized projectors, called "ortho-atomic", are compared to results from the exact formulae. Panels a) and b) of Figure 1 show a perfect agreement between the results for the two sets of projectors applied for the  $d$ -shell, ensuring us that the applied approximation for the derivatives in forces is rather good.

In panels c) and d) of Figure 1, the pSIC results are presented for the same atomic displacements which have been described above for the LDA+U method. As one can see, the force vanishes exactly at the geometry that coincides with the atomic position for which the total energy gets the minimum. It clearly demonstrates the correctness of the equations for forces derived for the pSIC method in this paper.

Next, a relaxation of the displaced atomic positions within the wurzite ZnO cell has been performed within the Newton-Raphson optimization scheme based on the Broyden-Fletcher-Goldfarb-Shanno (BFGS) algorithm<sup>24</sup> for the estimate of the inverse Hessian matrix. The criteria for the geometry optimization have been set as: the energy difference between subsequent BFGS-steps  $< 10^{-4}$  Ry, and the force  $< 10^{-3}$  Ry/a.u.

The starting non-equilibrium geometry has been obtained by application of the same distortion for all calculations: the LDA, the LDA+U, and the pSIC. The wurzite structure has been perturbed in a such way that two " $u$ " parameters (that determine the Zn-O distances along the  $z$ -axis and are defined as the bond length along the hexagonal symmetry axis devised by the lattice constant  $c$ ) for the Wyckoff positions have been chosen for the Zn-O distances along the  $z$ -axis: to be equal to  $u_1=0.349$  and  $u_2=0.412$ , which corresponds to considerably shorter and longer bond lengths, respectively (for the perfect wurzite structure  $u_1=u_2$ ). The lattice constant has been optimized for each method prior to the relaxation. The identical initial distorted geometry has been used to find the equilibrium geometry within the LDA, LDA+U, and pSIC approaches.

The results are displaced in Table I that collects the optimized lattice constants, the Zn-O bond lengths along the  $z$ -axis for the distorted and relaxed structures, and the optimized  $u$  parameters. For all three methods, the optimized  $u$  parameters (i.e.,  $u_1$  and  $u_2$ ) are identical. This correct result strongly corroborates the correctness of the derived equations for forces in the pSIC scheme. Note also that the lattice constant  $c$  obtained in pSIC method agrees better with the experimental value (9.83 a.u.) than the lattice constants obtained in the LDA and the LDA+U schemes.

As the next test case for the equations for forces, we consider a rare earth compound  $CeO_2$  in the  $F_{m3m}$  structure.<sup>26</sup> Here, we have chosen for the calculations

	Exp.	LDA	LDA+U	pSIC
lattice constant $a$	6.16	6.04	6.05	6.09
lattice constant $c$	9.84	9.68	9.70	9.76
<b>starting distorted geometry</b>				
Zn(1)-O(1)	-	3.382	3.388	3.410
Zn(2)-O(2)	-	3.986	3.993	4.019
<b>relaxed parameters</b>				
$u$ parameter	0.382	0.381	0.381	0.379
Zn-O bond	3.759	3.684	3.691	3.697

TABLE I. The geometry parameters of initially distorted and fully relaxed wurzite ZnO, calculated with the LDA, the LDA+U and the pSIC methods; obtained with the BFGS algorithm which contains forces. Lattice constants and bond lengths are in a.u. The experimental values are from Ref. [25].

the USPP, the Perdew-Zunger LDA functional, the kinetic energy cutoff of 35 Ry, and the uniform (8,8,8) Monkhorst-Pack  $k$ -mesh.

In Figure 2, the total energy and the force acting on the displaced atom Ce(1) are shown. The atom is displaced only along the  $[1,1,0]$  crystal-axis and the magnitude of the displacement is given as a function of Wyckoff position in units of the lattice constant, which has been fixed for this test at the experimental value of 5.41 a.u. The total energy minimum and the zero force occur exactly at the equilibrium geometry of the non-distorted structure. This is a next proof for the derived force formulae, which work also for the  $f$ -electron compound. For a comparison, we have also presented approximate forces which have been obtained neglecting the derivatives with respect to the atomic position of the occupation numbers. Such terms enter equations (10–12), and they were omitted in Refs. [12,18]. However, similar terms are present in the DFT+U forces.<sup>21</sup> In these two cases, the forces slightly differ, but both approaches give zero force at the same geometry.

## B. Distorted perovskites: $LaTiO_3$ , $YTiO_3$ , $LaMnO_3$

Strongly correlated perovskites  $LaTiO_3$ ,  $YTiO_3$ , and  $LaMnO_3$  exhibit Jahn-Teller distortions and crystallize in the  $P_{nma}$  structure.<sup>26</sup> They have been widely studied within the DFT+U method, just to mention as an example the work by Okatov *et al.*<sup>27</sup> (for  $LaTiO_3$  and  $YTiO_3$ ), and by Trimarchi and Binggeli<sup>28</sup> (for  $LaMnO_3$ ).

Nevertheless, the self-interaction correction applied to the oxygen atom in these compounds may cause some changes in the predicted geometry in comparison to the DFT+U results.

At low temperatures,  $LaTiO_3$  has a G-type antiferro-

Atom	Class	Coordinated
RE,O <sub>1</sub>	4c	$(u,1/4,v), (\bar{u}+1/2,3/4,v+1/2)$ $(\bar{u},3/4,\bar{v}), (u+1/2,1/4,\bar{v}+1/2)$
TM	4a	$(0,0,0), (1/2,0,1/2)$ $(0,1/2,0), (1/2,1/2,1/2)$
O <sub>2</sub>	8d	$\pm(x,y,z)$ $\pm(\bar{x},\bar{y},z)+(1/2,0,1/2)$ $\pm(\bar{x},y,\bar{z})+(0,1/2,0)$ $\pm(x,\bar{y},\bar{z})+(1/2,1/2,1/2)$

TABLE II. The Wyckoff positions for each ionic specie in the  $Pnma$  structure of RETMO<sub>3</sub> (RE=La,Y and TM=Ti,Mn).

magnetic structure and YTiO<sub>3</sub> is a ferromagnet, while a colossal magnetoresistance material LaMnO<sub>3</sub> is an A-type antiferromagnet. It is known that relations between the cell-axes determine the magnetic order in distorted perovskites. However, the calculation of stress tensor is not implemented yet in the pSIC approach. Therefore, we focus on the FM-ordered structures keeping the cell parameters fixed at the room-temperature crystallographic data. The details of the  $Pnma$  crystal structure are given in the Table II. For such cell, we optimized the geometry employing various DFT schemes, namely the GGA, the GGA+U, and the pSIC.

For all schemes, we have chosen the Perdew-Burke-Ernzerhof functional and employed the ultrasoft pseudopotentials. In the case of the GGA+U, the Hubbard-U parameter for Ti and Mn was set to 3.0 eV. In the pSIC calculations, the self-interaction correction has been applied to the outermost  $d$ -shell of rare-earth (RE) and transition-metal (TM) elements and also to the  $2s$ - and  $2p$ -shells of the oxygen. The results of calculation within the GGA, the GGA+U, and the pSIC methods are collected in Table III, which presents crystallographic parameters obtained from the BFGS optimization and compares them to the experimental data.

As one can see, the distortions calculated with the pSIC method are usually larger than obtained from the GGA and the GGA+U methods. Most of structural parameters calculated within the pSIC method are closer to the GGA+U numbers than to the GGA ones. Nevertheless, inclusion of the self-interaction correction to the  $2s$  and  $2p$  shells of the oxygen leads to a substantial difference, and brings the pSIC results usually closer to the experimental values. Some discrepancies still exist, especially for small parameters, and their reasons may lay on the accuracy of either the theoretical methods or experimental techniques. On the theoretical side, for example, the reported calculations involve the pseudopotentials and it is an open question how obtained results would differ from the results of all-electron approach.

Table III gives also the mean error of the calculated parameters  $P^M$  with respect to the experimental values

Parameters	Exp.	GGA	GGA+U	pSIC
<b>LaTiO<sub>3</sub></b>				
Exp. <sup>29</sup> a=10.6647 a.u., b=14.9300 a.u., c=10.5607 a.u.				
RE $u$	0.4916	0.4635	0.4685	0.4734
RE $v$	0.0457	-0.0014	-0.0019	-0.0107
O <sub>1</sub> $u$	0.0799	0.0163	0.0330	0.0609
O <sub>1</sub> $v$	0.0087	-0.0464	-0.0862	-0.0877
O <sub>2</sub> $x$	0.2096	0.2022	0.1938	0.1997
O <sub>2</sub> $y$	0.0417	0.0259	0.0400	0.0374
O <sub>2</sub> $z$	0.2941	0.2920	0.3124	0.3317
<b>YTiO<sub>3</sub></b>				
Exp. <sup>30</sup> a=10.0375 a.u., b=14.3827 a.u., c=10.7318 a.u.				
RE $u$	0.4793	0.4486	0.4317	0.4633
RE $v$	0.0729	-0.0076	0.0131	-0.0109
O <sub>1</sub> $u$	0.1211	0.0268	0.0266	0.0558
O <sub>1</sub> $v$	0.0042	-0.0980	-0.1227	-0.0921
O <sub>2</sub> $x$	0.1910	0.1852	0.1864	0.1791
O <sub>2</sub> $y$	0.0580	0.0470	0.0642	0.0358
O <sub>2</sub> $z$	0.3100	0.3114	0.3062	0.3449
<b>LaMnO<sub>3</sub></b>				
Exp. <sup>31</sup> a=10.8508 a.u., b=14.4904 a.u., c=10.4540 a.u.				
RE $u$	0.5490	0.5525	0.5536	0.5524
RE $v$	0.0100	0.0097	0.0101	0.0093
O <sub>1</sub> $u$	-0.0140	-0.0211	-0.0232	-0.0255
O <sub>1</sub> $v$	-0.0700	-0.0834	-0.0910	-0.0791
O <sub>2</sub> $x$	0.3090	0.2990	0.3068	0.3192
O <sub>2</sub> $y$	0.0390	0.0434	0.0458	0.0436
O <sub>2</sub> $z$	0.2240	0.2144	0.2180	0.2274
<b>Mean error <math>\langle \Delta \rangle</math></b>				
RE $u$	-	0.13	0.16	0.08
RE $v$	-	2.24	1.65	2.37
O <sub>1</sub> $u$	-	2.08	2.02	1.60
O <sub>1</sub> $v$	-	30.86	41.42	34.14
O <sub>2</sub> $x$	-	0.10	0.11	0.14
O <sub>2</sub> $y$	-	0.68	0.32	0.60
O <sub>2</sub> $z$	-	0.05	0.10	0.25

TABLE III. Experimental and theoretical parameters of  $Pnma$  structure (in crystal coordinates) for LaTiO<sub>3</sub>, YTiO<sub>3</sub> and LaMnO<sub>3</sub>, obtained from the BFGS relaxation within the GGA, the GGA+U, and the pSIC methods. Last block in the table gives the mean error of parameters obtained with each method in comparison to the experimental values (defined by eq. (13)).

$P^{Exp}$ ; it is defined as

$$\langle \Delta \rangle = \sum_{struct.} \left| \frac{P^M - P^{Exp}}{P^{Exp}} \right|, \quad (13)$$

where the summation runs over all calculated structures: LaTiO<sub>3</sub>, YTiO<sub>3</sub>, LaMnO<sub>3</sub>. One general observation is clear: the smaller is the parameter, the larger is the discrepancy between the calculated and the experimental values. Generally the distortions from the ideal perovskite structure are larger in the calculations than in the experiment. This might be due to the fact that, in

	pair 111		pair 220	
	TM-TM	TM-Si	TM-TM	TM-Si
ideal Si geom.	4.4686	4.4686	7.2983	4.4686
GGA, TM=Mn	4.8132	4.5202	7.1868	4.4871
pSIC, TM=Mn	4.9495	4.5429	7.2735	4.5552
GGA, TM=Re	4.1837	4.5532	5.7524	4.4768
pSIC, TM=Re	4.1713	4.5181	6.5140	4.4108

TABLE IV. The distances TM-TM and TM-Si (in Bohr) in Si:Mn and Si:Re for two configurations of impurities: 111 and 220 obtained after the BFGS minimization from the GGA and the pSIC approaches.

the experiment, the signal is averaged over the sample, which is never clean and so ideally periodic like in the calculations.

Concerning the FM-order, all theoretical methods give the magnetic moments of the Ti atom equal to  $1.0 \mu_B$  in both  $\text{LaTiO}_3$  and  $\text{YTiO}_3$ , whereas the calculated magnetic moment at Mn in  $\text{LaMnO}_3$  is  $4.0 \mu_B$ . Discussion of magnetic structure issues runs beyond the scope of this work, however, we would like to mention that the results obtained in this paper agree with numbers calculated within the GGA and the GGA+U schemes and reported earlier by other authors.<sup>27</sup>

### C. Diluted magnetic semiconductors: Si:Mn and Si:Re

As the third example, we have chosen two prototypes of the DMS systems. We consider the silicon crystal doped (i) with two Mn, and (ii) two Re impurities per cell. Detailed investigations of structural and magnetic properties of these DMS's will be given elsewhere. Here, we only present an effect of the pSIC scheme on the geometry around the transition-metal ions (TM) by comparing the atomic positions obtained from the pSIC and the standard GGA method. We consider two geometries of the TM pairs substituted into Si sites within the cubic unit cell with 64 atoms (with the silicon lattice constant resulting from the GGA calculations and equal to 10.32 a.u.). We consider (i) two TM atoms being the nearest neighbors (hereafter indicated as 111, since they take the sites (000) and  $a/4(111)$  in the silicon crystal, where  $a$  is the silicon lattice constant) and (ii) two TM atoms in the next nearest neighbours sites, they are bridged by the Si atom (hereafter indicated as 220, since they occupy the sites (000) and  $a/4(220)$ ).

Table IV presents the distances between: (i) transition-metal ions (TM-TM), and (ii) the transition metal and the silicon atom adjacent to the one of the TM-ions (for 111), and (iii) the TM-ion and the Si atom at the bridge

TM-Si-TM (for 220); obtained from the BFGS minimization performed in the GGA and the pSIC schemes, and compared to the ideal geometry of the silicon crystal.

In the case of the close distance pairs (111), the Mn ions repel themselves, while the Re ions attract each other in comparison to distances in the ideal silicon crystal. This effect is considerably stronger in the pSIC than in the GGA method.

For the 220 pairs, the TM ions get closer in the both cases of Mn-Mn and Re-Re pairs, the effect being especially pronounced for Re ions. In contrast to the 111 case, this attraction of TM pairs effect is much weaker in the pSIC than in the GGA approach. The TM-Si distances usually become slightly longer than the ideal Si-Si bond, except for the Re-Si-Re bridge in the pSIC approach. This effect is important for the magnetic properties of silicon doped with Re and will be published elsewhere. Here, we only comment on the fact that, the rhenium ions in silicon have smaller magnetic moment ( $1 \mu_B$ ) than the Mn ions ( $3 \mu_B$ ), and therefore, rhenium employs more valence electrons for a hybridization with atoms of the host and with another close Re ion. Due to a larger localization of the d-shell electrons in Re within the pSIC approach, these states contribute much weaker to a hybridization between Re-Re, and this bond is much longer than in the GGA method. A very interesting difference between Si:Mn and Si:Re is in the DOS: the states, which are closer to the Fermi level, originate from the closest neighbours of the impurity in the case of Mn, and from the second close neighbours in the case of Re. This fact gives one of the reasons why the 220 pair of Re in Si relaxes stronger than the 111 pair.

## V. SUMMARY

We have derived the expressions for forces within the non-variational pSIC approach with ultrasoft pseudopotentials used to account for electron and ion interactions and implemented the scheme into the QUANTUM ESPRESSO plane-wave code. First, we have performed benchmark calculations to check the internal consistency of the scheme for the wurzite ZnO and rare-earth  $f$ -electron compound  $\text{CeO}_2$  in the  $F_{m3m}$  structure. In both cases, the forces within the pSIC scheme vanish for the geometry corresponding to the minimum of the total energy. Also optimization procedure within the code works perfectly bringing the initially distorted crystallographic structures of ZnO and  $\text{CeO}_2$  into the correct equilibrium geometry efficiently.

Further, we have performed calculation within the pSIC approach to determine the geometry of distorted perovskites  $\text{LaTiO}_3$ ,  $\text{YTiO}_3$ , and colossal magnetoresistance compound  $\text{LaMnO}_3$  in the  $P_{nma}$  structure, and also of silicon doped with pairs of Mn and Re ions. These systems have been chosen, since there are indications that the spurious self-interaction and resulting more diffused electronic states can lead to certain systematic errors.

Indeed, in the cases studied here, the pSIC results for geometry parameters are usually closer to the experimental ones than the parameters obtained from the standard approximations of the DFT and the DFT+U methods. This strongly suggests that the larger localization of the electronic states is better accounted for in the pSIC scheme, which could provide also more reliable predictions in many systems. Also in the case of Mn and Re pairs in silicon, the geometries of the systems obtained within the pSIC and the GGA differ considerably. Effect of the pSIC relaxations is usually weaker than the GGA ones, which is a consequence of weaker *sp-d* hybridization. An exception is the Re-Si-Re configuration for which the Re1(5d)-Re2(5d) interactions are strong and the pSIC relaxations are larger than those obtained from the GGA method.

Having functioning scheme to calculate forces within the pSIC method, the further studies are under way to determine the areas of relevant applications and deeper investigate the reliability of the method.

## VI. ACKNOWLEDGMENTS

We would like to thank Andrzej Fleszar for numerous valuable discussions. M.W. acknowledges the support of the Leibniz Supercomputing Centre in Munich, where all the benchmarks have been run. The work was supported by the European Funds for Regional Development within the SICMAT Project (Contract No. UDA-POIG.01.03.01-14-155/09).

### Appendix A: Derivatives of the orbital occupation numbers with respect to the ionic displacement

Partial derivatives of the occupation numbers,  $p_{I,m_l,m_l',l}^\sigma$ , with respect to the atomic displacements,  $\tau_{\alpha,I}$ , are given in Ref. [21] by eqs. (13-19). Nevertheless, for the completeness, we include these derivations here.

We start from the occupation numbers in the norm-conserving pseudopotential scheme.

$$\frac{\partial p_{I,m_l,m_l',l}^\sigma}{\partial \tau_{\alpha,I}} = \sum_{n,\mathbf{k}} f_{n\mathbf{k}}^\sigma \left[ \frac{\partial}{\partial \tau_{\alpha,I}} (\langle \psi_{n\mathbf{k}}^\sigma | \phi_{I,m_l,l} \rangle) \langle \phi_{I,m_l,l} | \psi_{n\mathbf{k}}^\sigma \rangle + \langle \psi_{n\mathbf{k}}^\sigma | \phi_{I,m_l,l} \rangle \frac{\partial}{\partial \tau_{\alpha,I}} \langle \phi_{I,m_l,l} | \psi_{n\mathbf{k}}^\sigma \rangle \right].$$

The derivative of  $\langle \psi_{n\mathbf{k}}^\sigma | \phi_{I,m_l,l} \rangle$  reduces to the derivative of  $\phi_{I,m_l,l}$ , since due to Hellman-Feynman theorem  $\psi_{n\mathbf{k}}^\sigma$  does not change with the displacement.

The atomic orbitals  $\phi_{I,m_l,l}$  are represented in the plane-wave basis at each vector  $\mathbf{k}$  from the IBZ, in order to project them onto the Bloch functions. Then, the projection is symmetrized, to take care of the summation over all points from the BZ. The atomic orbital at point  $\mathbf{k}$  is expressed:

$$\phi_{I,m_l,l,\mathbf{k}}(\mathbf{r}) = \frac{1}{\sqrt{N}} \sum_{\mathbf{R}} e^{-i\mathbf{k}\cdot\mathbf{R}} \phi_{I,m_l,l}(\mathbf{r} - \mathbf{R} - \boldsymbol{\tau}_I) = e^{-i\mathbf{k}\cdot\mathbf{r}} \frac{1}{\sqrt{N}} \sum_{\mathbf{R}} e^{-i\mathbf{k}(\mathbf{r}-\mathbf{R})} \phi_{I,m_l,l}(\mathbf{r} - \mathbf{R} - \boldsymbol{\tau}_I).$$

$N$  is the number of the direct lattice vectors  $\mathbf{R}$ . The function  $\phi_{I,m_l,l}(\mathbf{r} - \mathbf{R} - \boldsymbol{\tau}_I)$  is periodic with the lattice and its Fourier expansion in the reciprocal lattice vectors  $\mathbf{G}$  is defined as:

$$\phi_{I,m_l,l}(\mathbf{r}) = \frac{1}{\sqrt{V}} \sum_{\mathbf{G}} e^{-i(\mathbf{k}+\mathbf{G})\cdot\mathbf{r}} c_{I,m_l,l}(\mathbf{k} + \mathbf{G}),$$

where  $V$  is the volume of the system ( $V=N\Omega$  and  $\Omega$  is the cell volume). The Fourier components  $c_{I,m_l,l}(\mathbf{k} + \mathbf{G})$  read:

$$c_{I,m_l,l}(\mathbf{k} + \mathbf{G}) = \frac{1}{\sqrt{V}} \int d\mathbf{r} e^{i(\mathbf{k}+\mathbf{G})\cdot\mathbf{r}} \phi_{I,m_l,l}(\mathbf{r}) = \frac{1}{N\sqrt{\Omega}} \sum_{\mathbf{R}} \int d\mathbf{r} e^{i(\mathbf{k}+\mathbf{G})(\mathbf{r}-\mathbf{R})} \phi_{I,m_l,l}(\mathbf{r} - \mathbf{R} - \boldsymbol{\tau}_I) = \frac{1}{N\sqrt{\Omega}} e^{i(\mathbf{k}+\mathbf{G})\cdot\boldsymbol{\tau}_I} \sum_{\mathbf{R}} \int d\mathbf{r} e^{i(\mathbf{k}+\mathbf{G})\cdot\mathbf{r}} \phi_{I,m_l,l}(\mathbf{r}).$$

The derivative of the atomic function  $\phi_{I,m_l,l}$  with respect to the displacement of the same atom I in the direction  $\alpha$  is thus

$$\frac{\partial \phi_{I,m_l,l}}{\partial \tau_{\alpha,I}} = \frac{i}{\sqrt{V}} \sum_{\mathbf{G}} e^{i(\mathbf{k}+\mathbf{G})\cdot\mathbf{r}} c_{I,m_l,l}(\mathbf{k} + \mathbf{G}) (\mathbf{k} + \mathbf{G})_\alpha,$$

where  $(\mathbf{k} + \mathbf{G})_\alpha$  is the vector component along the polarization  $\alpha$ .

The derivatives of the occupation numbers in the norm-conserving pseudopotential scheme are nonvanishing only for the displacement of the same atom at which the occupations are considered.

In the ultrasoft-pseudopotential scheme, the derivatives  $|\partial(\hat{S}\phi_{I,m_l,l})/\partial\tau_{\alpha,I}\rangle$  have to be computed. According to eq. (8), the above derivative contains derivatives of the  $\beta_\alpha$  functions (here the index  $\alpha = [n, l, m, I]$ ). These functions are the ultrasoft pseudopotential functions, which can be expressed also in the plane-wave representation. The overlap given by eq. (8) is nonlocal in  $\beta_\alpha$ . Therefore, we made the approximation mentioned in section III, and we neglected contributions from the derivatives of the  $\beta_{\alpha'}$  functions centred at atoms I' different than the moved atom I.



- 
- <sup>1</sup> P. Hohenberg and W. Kohn, Phys. Rev. **136**, B864 (1964); W. Kohn and L. J. Sham, Phys. Rev. **140**, A1133 (1965).
- <sup>2</sup> A. Görling, Phys. Rev. B **53**, 7024 (1996); **59**, 10370(E) (1999).
- <sup>3</sup> M. Städele, J. A. Majewski, P. Vogl, and A. Görling, Phys. Rev. Lett. **79**, 2089 (1997); M. Städele, M. Moukara, J. A. Majewski, P. Vogl, and A. Görling, Phys. Rev. B **59**, 10031 (1999).
- <sup>4</sup> J. B. Krieger, Y. Li, G. J. Yafrate, Phys. Lett. A **146**, 256 (1990).
- <sup>5</sup> V.I. Anisimov, J. Zaanen, and O.K. Andersen, Phys. Rev. B **44**, 943 (1991); V.I. Anisimov, F. Aryasetiawan, and A.I. Lichtenstein, J. Phys.: Condens. Matter **9**, 767 (1997).
- <sup>6</sup> J. P. Perdew and A. Zunger, Phys. Rev. B **23**, 5048 (1981).
- <sup>7</sup> A. Svane, O. Gunnarsson, Phys. Rev. Lett. **65**, 1148 (1990).
- <sup>8</sup> Z. Szotek, W. M. Temmerman, H. Winter, Phys. Rev. B **47**, 4029 (1993).
- <sup>9</sup> M. Arai, T. Fujiwara, Phys. Rev. B **51**, 1477 (1995).
- <sup>10</sup> D. Vogel, P. Krüger, J. Pollmann, Phys. Rev. B **54**, 5495 (1996).
- <sup>11</sup> A. Filippetti and N. A. Spaldin, Phys. Rev. B **67**, 125109 (2003).
- <sup>12</sup> A. Filippetti and V. Fiorentini, Eur. Phys. J. B **71**, 139 (2009).
- <sup>13</sup> A. Filippetti, N. A. Spaldin, and S. Sanvito Chem. Phys. **309**, 59, (2004).
- <sup>14</sup> M. Toyoda, H. Akai, K. Sato, H. Katayama-Yoshida, Physica B **376-377**, 647 (2006).
- <sup>15</sup> D. Puggioni, A. Filippetti, V. Fiorentini, Phys. Rev. B **79**, 064519 (2009).
- <sup>16</sup> C. D. Pemmaraju, T. Archer, D. Sánchez-Portal, and S. Sanvito Phys. Rev. B **75**, 045101 (2007).
- <sup>17</sup> C. Toher, A. Filippetti, S. Sanvito, and Kieron Burke, Phys. Rev. Lett. **95**, 146402 (2005).
- <sup>18</sup> A. Filippetti, C. D. Pemmaraju, S. Sanvito, P. Delugas, D. Puggioni, and Vincenzo Fiorentini, Phys. Rev. B **84**, 195127 (2011).
- <sup>19</sup> P. Giannozzi et al., J. Phys. Condens. Matter, **21**, 395502 (2009).
- <sup>20</sup> D. Vanderbilt, Phys. Rev. B **41**, R7892 (1990).
- <sup>21</sup> M. Cococcioni, Rev. Mineral. and Geochem. **71**, 147 (2010).
- <sup>22</sup> L. Kleinman and D. M. Bylander, Phys. Rev. Lett. **48**, 1425 (1982).
- <sup>23</sup> H. D. Monkhorst and J. D. Pack, Phys. Rev. B **13**, 5188 (1976).
- <sup>24</sup> Roger Fletcher, *Practical Methods of Optimization*, John Wiley and Sons, Chichester, 2nd edition, 1987.
- <sup>25</sup> *Semiconductors Physics of Group IV elements and III-V Compounds*, edited by K. H. Hellwege and O. Madelung, Landolt-Börnstein, New Series, Group III, Vol.17, Pt.a (Springer, Berlin 1982); *Intrinsic Properties of Group IV Elements and III-V, II-VI, and I-VII Compounds*, edited by K. H. Hellwege and O. Madelung, Landolt-Börnstein, New Series, Group III, Vol.22, Pt.a (Springer, Berlin 1987).
- <sup>26</sup> <http://cst-www.nrl.navy.mil/lattice>
- <sup>27</sup> S. Okatov, A. I. Poteryaev and A. I. Lichtenstein, Europhys. Lett. **70**, 499 (2005).
- <sup>28</sup> G. Trimarchi and N. Binggeli, Phys. Rev. B **71**, 035101 (2005).
- <sup>29</sup> M. Cwik, T. Lorenz, J. Baier, R. Muller, G. Andre, F. Bouree, F. Lichtenberg, A. Freimuth, R. Schmitz, E. Muller-Hartmann, M. Braden, Phys. Rev. B **68**, 060401(R) (2003).
- <sup>30</sup> D. A. MacLean et al., J. Solid State Chem. **30**, 35 (1979).
- <sup>31</sup> J. B. A. A. Elemans, B. van Laar, K. R. van der Veen, and B. O. Loopsra, J. Phys. Chem. Solids **3**, 238 (1971).

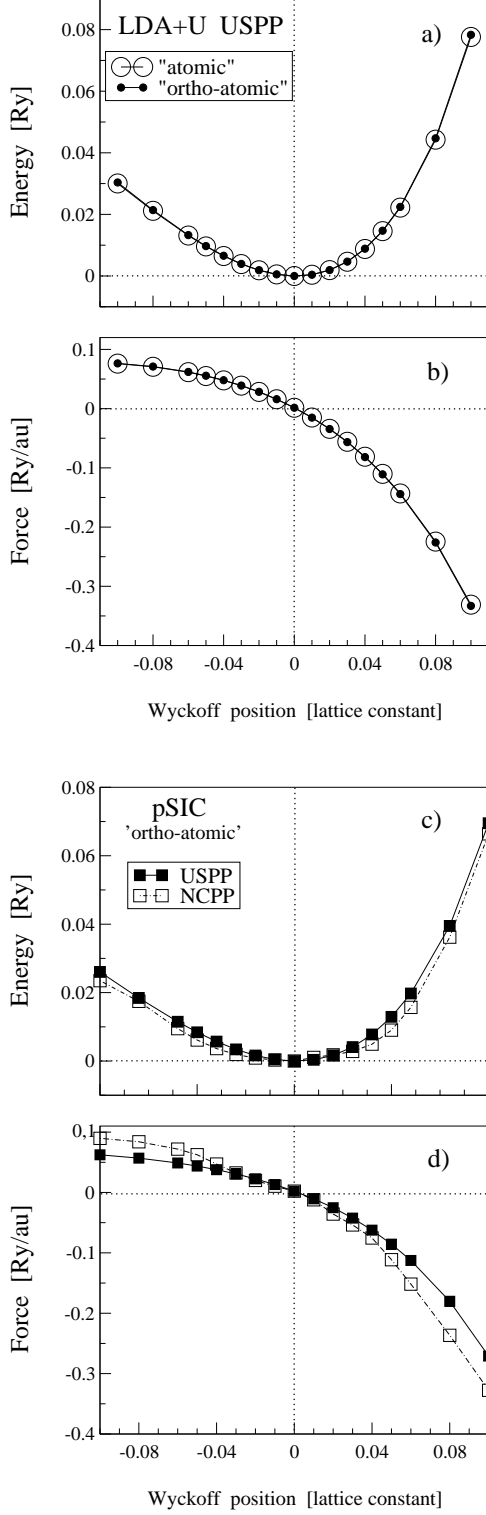


FIG. 1. Total energy of the wurzite ZnO and the force acting on the displaced atom Zn(1) along z-axis. Panels a) and b) are for the LDA+U ( $U=5$  eV) with "atomic" and "orthogonalized atomic" projectors for USPP, panels c) and d) are for the LDA+pSIC with "orthogonalized atomic" projectors for USPP and NCPP. Dotted lines are just guides for the eye.

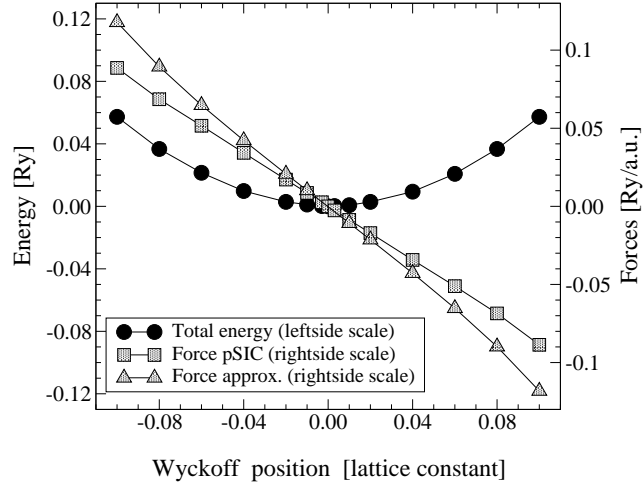


FIG. 2. Total energy of  $\text{CeO}_2$  in the  $F_{m3m}$  structure and the forces (according to our pSIC equations - squares, and approximated without terms containing the derivatives of the occupation numbers - triangles) acting on the atom Ce(1) displaced along the  $[1,1,0]$  crystal-direction; calculated with the USPP and the orthonormalized projectors.